ChemComm

COMMUNICATION

View Article Online
View Journal | View Issue

Cite this: *Chem. Commun.*, 2015, **51**, 13842

Received 25th June 2015,
Accepted 22nd July 2015

DOI: 10.1039/c5cc05211d

www.rsc.org/chemcomm

Urchin-like Au@CdS/WO_3 micro/nano heterostructure as a visible-light driven photocatalyst for efficient hydrogen generation†

Xing-Liang Yin, Jie Liu, Wen-Jie Jiang, Xing Zhang, Jin-Song Hu* and Li-Jun Wan

Urchin-like micro/nano heterostructure Au@CdS/WO_3 was synthesized by using a facile photodeposition method with no need for an additional stabilizer, which can be used as an efficient all-solid Z-scheme visible-light photocatalyst for H_2 generation with a high H_2 evolution rate.

Hydrogen, which possesses the highest energy density (142 MJ kg^{-1}) known for any fuel and no carbon emission,[1] is regarded as one of the most promising materials for future energy consumption. Among all the methods for hydrogen production, photocatalytic water splitting is the leading contender and will contribute to the upcoming energy revolution. Since 1972,[2] the research on semiconductor photocatalysts has made considerable progress, and a variety of materials were proved to be capable of producing hydrogen and/or oxygen. CdS-based photocatalysts[3–6] have been studied intensively because their electronic structures match well with the redox potential of splitting water into hydrogen and oxygen molecules. But the utilization of CdS is limited by photocorrosion and low activity which originate from inefficient electron and hole separation and transportation. Several measures including modifying surface defects,[7] loading cocatalysts,[8–10] tuning morphology,[11] or constructing heterojunctions[12] were taken to cover this limitation. Solid-state Z-scheme heterostructure photocatalysts[13–16] with two photocatalyst components have recently attracted increasing attention because they can effectively reduce the electron–hole recombination. However, previous research mainly focused on TiO_2[16] or ZnO[15] with photoactivity only under UV irradiation. Although doping was demonstrated to be an effective method to extend the photoresponse of the above-mentioned materials to visible light,[13,14] it will introduce new electron–hole recombination centers. In addition, few reports have shown that the morphology of the photocatalysts significantly affects light harvesting, charge transport, kinetic, power conversion efficiency and durability of the materials.[17]

As a photocatalyst, tungsten trioxide (WO_3) with a relatively narrow band gap (2.6 eV) has shown outstanding performance on restraining photocorrosion effects in aqueous solution.[18–22] Herein, we reported a new all-solid Z-scheme hybrid photocatalyst with a unique micro/nano heterostructure, which was prepared by using urchin-like WO_3 microstructures as a carrier and sequentially *in situ* photodeposition of Au and CdS nanocrystals to form Au@CdS/U-WO_3. WO_3 was selected based on the fact that its bottom of the conduction band (CB) was located between the bottom of the CB and top of the valence band (VB) of CdS, which made it an ideal material to combine with CdS for Z-scheme photocatalysts. The catalyst design and the mechanism of photocatalytic H_2 evolution are schematically illustrated in Fig. 1. Under light irradiation, the electrons were excited upon the CB of WO_3 and CdS. The excited electrons at the CB of WO_3 will be subsequently transferred to Au due to their high work function, while the holes remain in the VB. These electrons will recombine with the holes injected from the

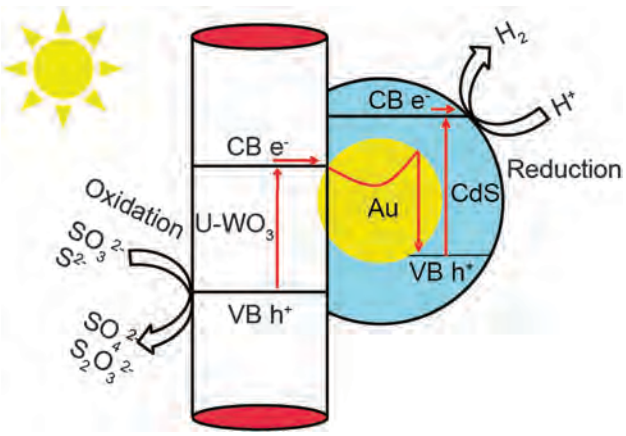

Fig. 1 Schematic illustration of the charge transfer in the Z-scheme photocatalyst Au@CdS/U-WO_3.

Beijing National Laboratory for Molecular Sciences, CAS Key Laboratory of Molecular Nanostructure and Nanotechnology, Institute of Chemistry, Chinese Academy of Science, 2 North 1st Street, Zhongguancun, Beijing 100190, China. E-mail: hujs@iccas.ac.cn

† Electronic supplementary information (ESI) available: Experimental section and supplementary figures. See DOI: 10.1039/c5cc05211d

VB of CdS to Au, reducing the probability of the recombination of electrons and holes in CdS. Therefore, more electrons at the CB of CdS can effectively involve in reducing H^+ into H_2, thus enhancing the H_2 evolution rate. The one-dimensional whiskers of urchin-like WO_3 facilitates the hole transfer and separation for the oxidation reaction. The three-dimensional micro-/nanostructure of the catalyst not only keeps the building blocks at the nanometer scale with the relatively large surface for the efficient deposition of nanocrystals, but also prevents the agglomeration of the active nanocrystals and facilities the mass transfer and easy recycling. As a result, the Au@CdS/U-WO_3 exhibited excellent performance for photocatalytic hydrogen evolution.

As shown in Fig. 2a, a Au@CdS/U-WO_3 photocatalyst was prepared by *in situ* loading Au nanocrystals onto the whiskers of urchin-like WO_3 micro-/nanostructures (U-WO_3) *via* photodeposition, followed by the growth of CdS nanoshells onto Au *via* photoreduction. In brief, U-WO_3 was first synthesized through a modified solvothermal process.[23] Au nanocrystals was *in situ* grown by illuminating the aqueous suspension containing U-WO_3 and $HAuCl_4$. The growth of CdS was initialized by illuminating the suspension containing the prepared Au/U-WO_3, S_8 and $Cd(ClO_4)_2$. Under irradiation, S_8 molecules were reduced to S^{2-} ions, which were then selectively adsorbed onto the surface of Au due to the strong affinity of Au atoms to sulphur.[24] In the presence of Cd^{2+} ions, the S^{2-} ions adsorbed onto the surface of Au reacted with Cd^{2+} and formed Au@CdS/U-WO_3. The experimental details are presented in the ESI.†

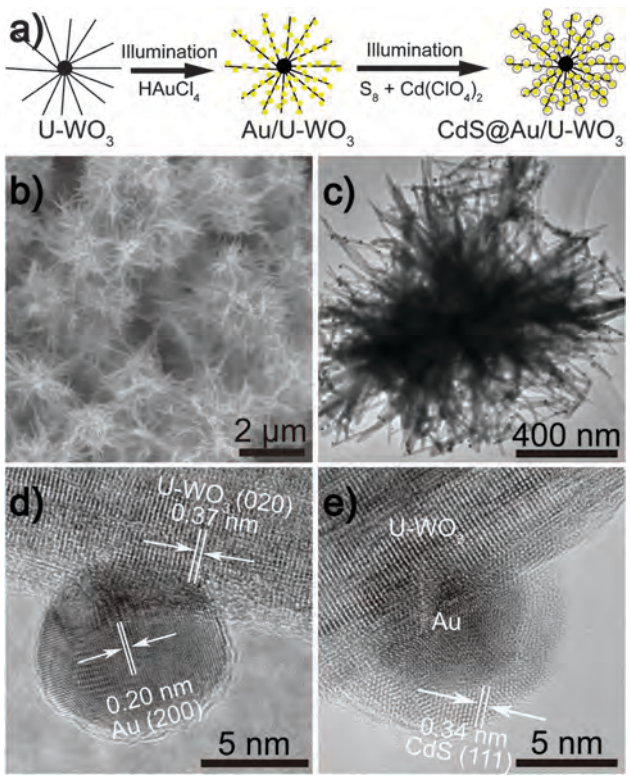

Fig. 2 (a) Scheme of the preparation of Au@CdS/U-WO_3; (b) SEM image of U-WO_3; (c) typical TEM image of Au/U-WO_3; (d and e) HRTEM images of Au/U-WO_3 (d) and Au@CdS/U-WO_3 (e).

The preparation details of each catalyst are listed in the ESI.† Fig. 2b shows the typical scanning electron microscopy (SEM) image of U-WO_3, showing urchin-like structures radially assembled by nanowire-like whiskers with an average length of about 1 μm. The low-magnification transmission electron microscopy (TEM) image (Fig. 2c) of the product after Au deposition (Au/U-WO_3) shows that the nanoparticles in darker contrast were grown on the surfaces of U-WO_3 whiskers. The high-resolution TEM image (HRTEM) shown in Fig. 2d clearly reveals the lattice fringes with a distance of 0.20 nm on the nanoparticles and that of 0.37 nm on the whiskers, which match well with the *d*-spacing of cubic Au(200) crystallographic planes and orthorhombic WO_3(020) planes, respectively. After the coating of CdS, the HRTEM image (Fig. 2e) shows that CdS was deposited on the surface of Au nanocrystals to achieve an Au@CdS core–shell nanostructure linked onto the surface of U-WO_3 (Au@CdS/U-WO_3). The distance of 0.34 nm among lattice fringes is in well agreement with the *d*-spacing of the (111) planes of wurtzite CdS.

The crystalline structures of the products at different stages (U-WO_3, Au/U-WO_3 and Au@CdS/U-WO_3) were further investigated by powder X-ray diffraction (XRD). XRD patterns are shown in Fig. 3a. All diffraction peaks of U-WO_3 can be attributed to orthorhombic WO_3 (JCPDS Card No. 20-1324). Compared with U-WO_3, the peaks at 38.2°, 44.4°, and 77.5° (marked with ●) appearing in the XRD pattern of Au/U-WO_3 can be ascribed to the diffraction from the (111), (200), (311) planes of cubic Au (JCPDS Card No. 04-0784), indicating that Au were successfully deposited on U-WO_3, which is consistent with the HRTEM result. The additional peaks at 26.5°, 43.9°, and 52.0° (marked with ■) in the XRD pattern of Au@CdS/U-WO_3 can be well indexed to the diffraction from the (111), (220), (311) planes of wurtzite CdS (JCPDS Card No. 65-2887), corroborating the existence of CdS.

UV-vis absorption spectra (Fig. 3b) of U-WO_3, Au/U-WO_3 and Au@CdS/U-WO_3 were recorded to examine their optical properties. Compared with the spectrum of U-WO_3, the spectrum of Au/U-WO_3 shows a broad shoulder peak centered at 530 nm, corresponding to the plasmonic absorption of Au nanoparticles.[25]

After the coating of CdS shells onto Au nanoparticles, this plasmonic resonance absorption shifted from 530 nm to 570 nm and broadened due to the strong electromagnetic coupling of Au and CdS.[26] The small shoulder peak appearing at 500 nm could be ascribed to the intrinsic absorption of CdS shells.[16] This result indicates the interaction between Au cores and CdS shells.

The photocatalytic activity of the prepared Au@CdS/U-WO_3 was evaluated by examining H_2 evolution *via* photocatalytic water-splitting under visible-light irradiation and compared with four control catalysts. The preparation details of control catalysts are listed in the ESI.† In brief, Au@CdS/C-WO_3 was prepared with the same procedure as Au@CdS/U-WO_3 but using commercial WO_3 instead of the prepared U-WO_3. Au/U-WO_3 and CdS/U-WO_3 were prepared without the step of CdS deposition or Au deposition, respectively. CdS was obtained by the same photodeposition procedure but without the addition of WO_3. (Au/U-WO_3, CdS) is the mixture of the above-mentioned

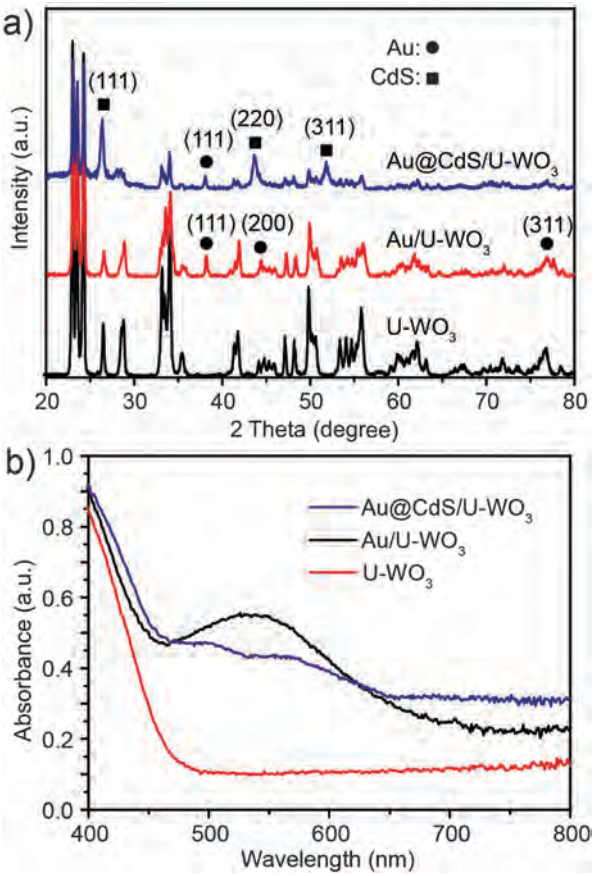

Fig. 3 (a) XRD patterns of U-WO_3, Au/U-WO_3 and Au@CdS/U-WO_3; (b) UV-vis absorption spectra of U-WO_3, Au/U-WO_3 and Au@CdS/U-WO_3.

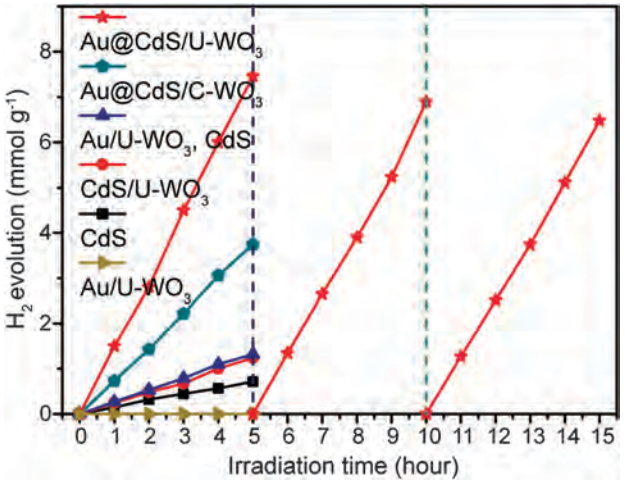

Fig. 4 Time courses of photocatalytic H_2 evolution on Au@CdS/U-WO_3, Au@CdS/C-WO_3, (Au/U-WO_3, CdS), CdS/U-WO_3 and CdS photocatalysts under visible-light irradiation ($\lambda > 420$ nm).

Table 1 The content of Au and CdS *versus* WO_3 measured by ICP-AES

Sample	1[a]	2[b]	3[c]	4[d]
Au : WO_3 (wt%)	1.93	1.17	2.01	
CdS[e] : WO_3 (wt%)	33.76	32.63		34.26

[a] Au@CdS/U-WO_3. [b] Au@CdS/C-WO_3. [c] Au/U-WO_3. [d] CdS/U-WO_3. [e] The contents of CdS were calculated based on the contents of Cd and S.

Au/U-WO_3 and CdS with a mass ratio of 3 : 1 to achieve the same content of CdS. The results of hydrogen evolution experiments are shown in Fig. 4. It can be clearly seen that Au@CdS/U-WO_3 demonstrated the highest H_2 evolution rate (1.39 mmol g^{-1} h^{-1}). The apparent quantum yield is 3.45%, which was calculated using the method shown in the ESI.† During the consecutive three runs over 15 h, Au@CdS/U-WO_3 did not show a substantial decrease in the photocatalytic activity. The very slight decrease could be ascribed to the loss of sacrificial reagents during the long-term reaction. In order to understand the role of Z-scheme design, the photocatalytic activity of Au@CdS/U-WO_3 was compared with those of Au/U-WO_3 and CdS/U-WO_3. It can be seen that Au/U-WO_3 did not show obvious catalytic activity, and the H_2 evolution rate of Au@CdS/U-WO_3 is 5.79 times higher than that of CdS/U-WO_3 (1.39 *vs.* 0.24 mmol g^{-1} h^{-1}). Furthermore, comparing Au@CdS/U-WO_3 with the physical mixture of (Au/U-WO_3 + CdS), the H_2 evolution rate of the former is 5.15 times higher than that of the latter (1.39 *vs.* 0.27 mmol g^{-1} h^{-1}). Taking into consideration the similar content of Au and CdS in the catalysts, which are determined by the inductively coupled plasma atomic emission spectroscopy (ICP-AES) and listed in Table 1, these results clearly revealed that the WO_3–Au–CdS Z-scheme design in Au@CdS/U-WO_3 significantly enhanced the photocatalytic activity of the catalyst for H_2 evolution.

Moreover, to reveal the role of urchin-like WO_3 support, the commercial granular WO_3 was used to prepare in parallel the Z-scheme photocatalyst (Au@CdS/C-WO_3). It can be seen from Fig. 4 that the Au@CdS/U-WO_3 exhibited almost two times higher H_2 evolution rate than the Au@CdS/C-WO_3 (1.39 *vs.* 0.73 mmol g^{-1} h^{-1}), indicating that the urchin-like three dimensional morphology of Au@CdS/U-WO_3 significantly contributed to the increase of the photocatalytic activity. This enhancement can be ascribed to the fact that the higher surface area of U-WO_3 led to the efficient loading of Au@CdS. Fig. S1 (ESI†) presents the isothermal adsorption–desorption curves and the corresponding pore-size distribution curves of U-WO_3 and C-WO_3. The results show that the Brunauer–Emmett–Teller (BET) surface area of U-WO_3 is 202.469 m^2 g^{-1}, which is much larger than that of C-WO_3 (0.778 m^2 g^{-1}). The higher surface area will allow loading more Au nanocrystals on WO_3 to obtain more photocatalytically active sites with a Z-scheme structure. This was corroborated by the higher Au content in Au@CdS/U-WO_3 (1.93 *vs.* 1.17 wt% of Au : WO_3). Furthermore, it could be assumed that the one-dimensional nanowire-like structure in Au@CdS/U-WO_3 benefited from the hole transfer during illumination and thus relieved the recombination of charge carriers.[27,28] It should be noted that the H_2 generation of all catalysts discussed here was measured in the presence of Na_2SO_3 and Na_2S as the sacrificial reductants which were commonly used in the evaluation of HER photocatalysts. Although the addition of these reductants will not affect the evaluation and comparison of photocatalysts for H_2 evolution

alone, the development of stable HER photocatalysts with no need for sacrificial reductants is important and urgent for water splitting but still very challenging.

In conclusion, a new all-solid hybrid photocatalyst Au@CdS/U-WO_3 with a unique urchin-like micro/nano heterostructure was designed and successfully prepared by the sequential photodeposition of Au and CdS on a WO_3 support with no need for additional additives. The results exhibited that the Z-scheme design in this catalyst significantly enhanced the photocatalytic activity for H_2 evolution. The urchin-like micro/nano morphology of the catalyst not only maintains the active component at the nanometer scale for high activity but also provides three-dimensional structure at the micrometer scale for facile mass transfer and easy recycling.

This work was supported by the National Key Project on Basic Research (2011CB808701, 2015CB932302), the National Natural Science Foundation of China (91127044 and 21173237), and the Strategic Priority Research Program of the Chinese Academy of Sciences (Grant No. XDB12020100).

References

1 F. Bonaccorso, L. Colombo, G. Yu, M. Stoller, V. Tozzini, A. C. Ferrari, R. S. Ruoff and V. Pellegrini, *Science*, 2015, **347**, 1246501.
2 A. Fujishima and K. Honda, *Nature*, 1972, **238**, 37–38.
3 X. Xu, C. Randorn, P. Efstathiou and J. T. S. Irvine, *Nat. Mater.*, 2012, **11**, 595–598.
4 C. A. Caputo, M. A. Gross, V. Lau, C. Cavazza, B. V. Lotsch and E. Reisner, *Angew. Chem., Int. Ed.*, 2014, **53**, 11538–11542.
5 L. Liao, Q. Zhang, D. Wei, Z. Su, G. Feng, F. Robles-Hernandez, Q. Yu, Z. Zhao, X. Cai, S. Baldelli and J. Bao, *Nat. Nanotechnol.*, 2013, **272**, 1–5.
6 T. Ohno, L. Bai, T. Hisatomi, K. Maeda and K. Domen, *J. Am. Chem. Soc.*, 2012, **134**, 8254–8259.
7 L. Huang, X. Wang, J. Yang, G. Liu, J. Han and C. Li, *J. Phys. Chem. C*, 2013, **117**, 11584–11591.
8 Q. Zhao, M. Ji, H. Qian, B. Dai, L. Weng, J. Gui, J. Zhang, M. Ouyang and H. Zhu, *Adv. Mater.*, 2014, **26**, 1387–1392.
9 T. Simon, N. Bouchonville, M. J. Berr, A. Vaneski, A. Adrović, D. Volbers, R. Wyrwich, M. Döblinger, A. S. Susha, A. L. Rogach, F. Jäckel, J. K. Stolarczyk and J. Feldmann, *Nat. Mater.*, 2014, **13**, 1013–1018.
10 X. Zong, H. Yan, G. Wu, G. Ma, F. Wen, L. Wang and C. Li, *J. Am. Chem. Soc.*, 2008, **130**, 7176–7177.
11 Y. Xu, W. Zhao, R. Xu, Y. Shi and B. Zhang, *Chem. Commun.*, 2013, **49**, 9803–9805.
12 K. Wu, Z. Chen, H. Lv, H. Zhu, C. L. Hill and T. Lian, *J. Am. Chem. Soc.*, 2014, **136**, 7708–7716.
13 H. J. Yun, H. Lee, N. D. Kim, D. M. Lee, S. Yu and a. J. Yi, *ACS Nano*, 2011, **5**, 4084–4090.
14 H. Zhou, L. Ding, T. Fan, J. Ding, D. Zhang and Q. Guo, *Appl. Catal., B*, 2014, **147**, 221–228.
15 Z. B. Yu, Y. P. Xie, G. Liu, G. Q. Lu, X. L. Ma and H.-M. Cheng, *J. Mater. Chem. A*, 2013, **1**, 2773.
16 H. Tada, T. Mitsui, T. Kiyonaga, T. Akita and K. Tanaka, *Nat. Mater.*, 2006, **5**, 782–786.
17 F. E. Osterloh, *Chem. Soc. Rev.*, 2013, **42**, 2294–2320.
18 P. M. Rao, L. Cai, C. Liu, I. S. Cho, C. H. Lee, J. M. Weisse, P. Yang and X. Zheng, *Nano Lett.*, 2014, **14**, 1099–1105.
19 B. M. Klepser and B. M. Bartlett, *J. Am. Chem. Soc.*, 2014, **136**, 1694–1697.
20 K. Maeda, M. Higashi, D. Lu, R. Abe and K. Domen, *J. Am. Chem. Soc.*, 2010, **132**, 5858–5868.
21 S. Anandan and M. Miyauchi, *Chem. Commun.*, 2012, **48**, 4323–4325.
22 D. D. Qin, C. L. Tao, S. A. Friesen, T. H. Wang, O. K. Varghese, N. Z. Bao, Z. Y. Yang, T. E. Mallouk and C. A. Grimes, *Chem. Commun.*, 2012, **48**, 729–731.
23 G. Xi, J. Ye, Q. Ma, N. Su, H. Bai and C. Wang, *J. Am. Chem. Soc.*, 2012, **134**, 6508–6511.
24 T. Kiyonaga, T. Mitsui, M. Torikoshi, M. Takekawa, T. Soejima and H. Tada, *J. Phys. Chem. B*, 2006, **110**, 10771–10778.
25 V. Subramanian, E. E. Wolf and P. V. Kamat, *J. Am. Chem. Soc.*, 2004, **126**, 4943–4950.
26 I. Honma, T. Sano and H. Komiyama, *J. Phys. Chem.*, 1993, **97**, 6692–6695.
27 X. Zhang, X. Lu, Y. Shen, J. Han, L. Yuan, L. Gong, Z. Xu, X. Bai, M. Wei, Y. Tong, Y. Gao, J. Chen, J. Zhou and Z. L. Wang, *Chem. Commun.*, 2011, **47**, 5804–5806.
28 J. Su, X. Feng, J. D. Sloppy, L. Guo and C. A. Grimes, *Nano Lett.*, 2011, **11**, 203–208.